Research Square

Preprints are preliminary reports that have not undergone peer review.
They should not be considered conclusive, used to inform clinical practice,
or referenced by the media as validated information.

Matrix Anisotropy Regulates EMT- Associated Plasticity and Responses to Therapeutic Gene Silencing in Triple- Negative Breast Cancer

Muge Molbay
Ludwig-Maximilians-Universität München
Gabriele Loiudice
Ludwig-Maximilians-Universität München
Emma Thompson
Ludwig-Maximilians-Universität München
Ignasi Forné
Ludwig- Maximilians-Universität München
Axel Imhof
Ludwig- Maximilians-Universität München
Olivia M. Merkel
olivia.merkel@lmu.de

Ludwig-Maximilians-Universität München

Research Article

Keywords: Extracellular matrix anisotropy, tumor-associated collagen signatures, mechanotransduction, MED27, epithelial-mesenchymal plasticity, siRNA delivery

Posted Date: November 18th, 2026

DOI: https://doi.org/10.21203/rs.3.rs-11768918/v1

License: This work is licensed under a Creative Commons Attribution 4.0 International License.
Read Full License

Additional Declarations: Competing interest reported. O.M.M. is a co-founder of RNhale GmbH, an SAB member for AMW GmbH, Corden Pharma International GmbH, and Coriolis Pharma GmbH and a consultant for AbbVie Deutschland GmbH and PARI Pharma GmbH on unrelated projects. The remaining authors declare that they have no competing interests.

Abstract

The architectural organization of the tumor extracellular matrix (ECM) critically governs breast cancer progression by providing directional cues that drive cellular plasticity and invasion. However, the transcriptional regulators that link tumor-associated matrix anisotropy to epithelial-mesenchymal transition (EMT) remain poorly defined. Here, we investigated how ECM alignment regulates EMT in triple-negative breast cancer (TNBC) using a collagen-I-coated electrospun poly(ε-caprolactone) (PCL) scaffold platform that recapitulates tumor-associated collagen signatures (TACSs). Culturing TNBC cells on aligned fibrous architectures promoted a mesenchymal phenotype characterized by reduced *CDH1* (E-cadherin) expression, elevated *VIM* (vimentin) and *CD44* expression, and global proteomic remodeling of cytoskeletal and adhesion networks. Integrative proteomic and transcriptional profiling identified Mediator complex subunit 27 (MED27) as a previously unrecognized, matrix architecture-responsive transcriptional regulator whose mRNA and protein abundance significantly increased on aligned fibers. To evaluate the functional role of MED27 within these distinct topographies, we delivered MED27-targeting siRNA using either Lipofectamine or CD44-targeted, hyaluronan-coated poly(β-amino ester) (HAP) polyplexes. Silencing MED27 modulated key EMT- and growth-associated transcripts, including EGFR, VIM, and CDH1, in a substrate-dependent manner and impaired collective cell migration in gap-closure assays. By linking TACS-like collagen alignment to MED27 upregulation, this study identified a novel mechano-transcriptional node in TNBC and demonstrated the utility of biomimetic 3D fiber platforms for evaluating microenvironment-informed RNA nanotherapies.

Background

Breast cancer remains a leading global health burden, accounting for approximately 2.43 million new diagnoses and 694,000 deaths worldwide in 2024 [1, 2]. Despite advances in molecular subtyping and targeted therapeutics, metastatic recurrence continues to drive mortality, particularly in triple-negative breast cancer (TNBC) which is an aggressive subtype lacking estrogen, progesterone, and HER2 receptors [3–5]. Accumulating evidence has demonstrated that the tumor microenvironment (TME) actively governs cancer progression, with physicochemical remodeling of the extracellular matrix (ECM) driving cellular plasticity, local invasion, and metastasis [6–9]. Beyond bulk matrix stiffness and viscoelasticity [9], the spatial topography of fibrillar collagen provides potent directional cues. Clinically, these architectural rearrangements are classified as tumor-associated collagen signatures (TACSs), wherein radially aligned collagen bundles at the tumor-stroma interface correlate with poor patient prognosis [10, 11]. Functionally, aligned collagen fibers facilitate contact-guided migration and directional persistence, creating preferential tracks for tumor cell dissemination [12–15]. Crucially, these physical cues intersect with epithelial-mesenchymal transition (EMT), a dynamic transcriptional program through which carcinoma cells lose apicobasal polarity, remodel cell-cell junctions, and acquire invasive traits [16–18].

To dissect the biological impact of TACS under defined in vitro conditions, our group previously developed collagen-I-coated electrospun poly(ε-caprolactone) (PCL) scaffolds that mimic isotropic

(randomly oriented) and anisotropic (aligned) fibrous topographies [19, 20]. Using breast cancer cell lines spanning the EMT spectrum, we showed that fiber alignment dictates cellular elongation and contact-guided migration in a manner dependent on the intrinsic EMT state [19]. However, while the morphological and migratory consequences of collagen alignment are well documented, the nuclear transcriptional hubs that translate fibrous matrix anisotropy into EMT-associated gene expression remain largely unknown.

Mediator complex subunit 27 (MED27), a structural and functional component of the multiprotein Mediator coactivator complex that bridges transcription factors to RNA polymerase II, represents a compelling candidate at this mechano-transcriptional interface. Recent studies have implicated MED27 as an oncogenic driver across multiple solid tumors. In breast cancer, Wang et al. demonstrated that MED27 promotes malignancy and stemness by transcriptionally activating Krüppel-like factor 4 (KLF4) [21]. Similarly, MED27 depletion suppresses metastasis, angiogenesis, and EMT in gastric and adrenocortical carcinomas via attenuation of Wnt/β-catenin signaling [22, 23]. Nevertheless, whether MED27 expression is dynamically regulated by the architectural organization of the tumor ECM and whether therapeutic silencing of MED27 can blunt matrix-induced EMT plasticity have not been investigated.

Here, we examine the interplay between TACS-mimicking fiber alignment, MED27 expression, and EMT plasticity in TNBC. Combining collagen-I-coated electrospun PCL scaffolds with proteomics and qPCR in MDA-MB-231 and MDA-MB-468 cells, we identified MED27 as an anisotropy-responsive subunit of the Mediator complex. Furthermore, because aligned fibers markedly upregulate the hyaluronic acid (HA) receptor CD44, we evaluated targeted MED27 knockdown using both conventional lipid transfection and CD44-directed, HA-coated poly(β-amino ester) (HAP) nanoparticles [24, 25]. Our findings establish a direct link between fibrillar matrix organization and MED27 expression, highlighting how biomimetic ECM models can uncover context-dependent transcriptional targets in TNBC.

Materials and methods

Materials

Poly(ε-caprolactone) (PCL; Mw = 80 kDa), 3-(trimethoxysilyl)propyl methacrylate (98%), anhydrous dichloromethane (DCM), anhydrous N,N-dimethylformamide (DMF), HEPES, formaldehyde solution (≥ 36%), 4',6-diamidino-2-phenylindole dihydrochloride (DAPI), 5(6)-carboxyfluorescein diacetate N-succinimidyl ester (CFSE), FluorSave™, recombinant RNase-free DNase I, Dulbecco's modified Eagle medium (DMEM), fetal bovine serum (FBS), penicillin–streptomycin (Pen/Strep), phosphate-buffered saline (PBS), trypsin–EDTA (0.05% and 0.25%), Accutase®, L-glutamine (200 mM), and dimethyl sulfoxide (DMSO) were purchased from Sigma-Aldrich (Taufkirchen, Germany).

ATTO 643 NHS ester was obtained from ATTO-TEC (Siegen, Germany). The LIVE/DEAD™ Cell Vitality Assay (Calcein AM/SYTOX™ Deep Red), Silencer™ Select EGFR siRNA (s563), Silencer™ Select MED27

siRNA (n311365), Alexa Fluor™ 488 NHS ester, Pierce™ BCA Protein Assay Kit, Lipofectamine™ 2000, SYBR™ Gold, Power SYBR™ Green PCR Master Mix, PureLink™ RNA Mini Kit, TaqMan™ Cells-to-CT™ 1-Step Kit, TaqMan™ Array Human Epithelial-Mesenchymal Transition 96-well plates (RATZ77T), Opti-MEM™, and MEM Non-Essential Amino Acids (100×) were purchased from Thermo Fisher Scientific (Darmstadt, Germany).

Human CD44 Pan-Specific Antibody and medium-molecular-weight hyaluronic acid (HA; 75–350 kDa, GLR004) were obtained from R&D Systems (Minneapolis, MN, USA). Round glass coverslips (13 mm diameter) were purchased from VWR (Ismaning, Germany). µ-Slide 8 Well high (80806), µ-Dish 35 mm high (81156), and Culture-Insert 4 Well µ-Dish 35 mm high (80466) were obtained from Ibidi GmbH (Gräfelfing, Germany). Rat-tail collagen I (sc-136154) was purchased from Santa Cruz Biotechnology (Dallas, TX, USA).

The scrambled negative control siRNA (sense: 5'-pCGUUAAUCGCGUAUAAUACGCGUat-3'; antisense: 3'-CAGCAAUUAGCGCAUAUUAUGCGCAUAp-5') was purchased from Integrated DNA Technologies (Leuven, Belgium). QuantiTect Primer Assays for GAPDH (QT00079247), SNAI1 (QT00010010), CDH1 (QT00080143), VIM (QT00095795), CD44 (QT00998333), EGFR (QT00999957), MED27 (QT02503046), CCND1 (QT00095256), KLF4 (QT00063469), and BIRC5 (QT01579270) were obtained from Qiagen (Hilden, Germany).

Hyaluronan-coated PBAE/siRNA polyplexes (HAP) were formulated as described by Loiudice et al. [25], using spermine-containing PBAE copolymers synthesized according to previously established protocols [26].

Cell Culture

The human TNBC cell lines MDA-MB-231 and MDA-MB-468 were obtained from the American Type Culture Collection (ATCC; Manassas, VA, USA) and maintained in a humidified incubator at 37°C. Both cell lines were routinely authenticated via short tandem repeat (STR) profiling against the International Cell Line Authentication Committee (ICLAC) database and verified to be mycoplasma-free.

MDA-MB-231 cells were cultured in high-glucose DMEM supplemented with 4 mM L-glutamine, 10% (v/v) FBS, and 1% (v/v) Pen/Strep under 5% CO_2. MDA-MB-468 cells were maintained in Leibovitz's L-15 medium supplemented with 2 mM L-glutamine, 10% (v/v) FBS, 36 mM $NaHCO_3$ (2% v/v of 1.8 M stock), 20 mM HEPES, and 1% (v/v) Pen/Strep, adapted to 5% CO_2 incubation. Unless otherwise specified, cells were seeded at 2 × 10^4 cells per well in 24-well plates or ibiTreat µ-Dishes, and at 1 × 10^4 cells per well in Ibidi µ-Slides and 4-well culture inserts. All experiments were performed in independent triplicates, each containing technical triplicates, unless stated otherwise.

Electrospun scaffold fabrication and collagen coating

Randomly oriented and aligned PCL fibrous scaffolds were fabricated using a custom electrospinning setup as previously described [19]. Briefly, PCL was dissolved at 200 g/L in DCM/DMF (40:60, v/v) and extruded through a 23-gauge blunt-end needle (30 mm) at a constant flow rate of 1 mL/h using a dual-channel high-voltage power supply (± 30 kV; iseg GmbH, Radeberg, Germany) at 21–23°C and 50–60% relative humidity. Voltages were maintained at + 13 kV at the needle tip and − 1 kV at the collector. Randomly oriented fibers were collected on a stationary plate at a working distance of 24 cm, whereas aligned fibers were collected on a rotating mandrel (100 mm diameter; 1800 rpm; Nanotec Electronic GmbH) at a distance of 23 cm.

The fibers were deposited directly onto 13 mm glass coverslips pretreated with 3-(trimethoxysilyl)propyl methacrylate. The scaffolds were dried under vacuum, UV-sterilized, and coated with rat-tail collagen I at a surface density of 2 µg/cm² prior to cell seeding.

Microscopy, fiber alignment quantification, and cell viability

The scaffold architecture was imaged using an EVOS M5000 microscope (Thermo Fisher Scientific) equipped with 10×, 20×, and 40× phase-contrast objectives. Fiber orientation coherence was quantified in Fiji/ImageJ using the OrientationJ plugin, where coherence values ≤ 0.2 defined isotropic (randomly oriented) matrices and values ≥ 0.5 confirmed anisotropic (aligned) matrices.

Cell viability on scaffolds was assessed using the LIVE/DEAD™ Cell Vitality Assay by incubating cells with Calcein AM (0.25 µM) and SYTOX™ Deep Red (1 µM) according to the manufacturer's protocol. Confocal laser scanning microscopy was performed on a Leica SP8 inverted microscope equipped with 40×/1.30 and 63×/1.40 oil-immersion objectives using LAS X software. For imaging of the cellular uptake of the scaffolds, the cells were transfected with AF647-labeled siRNA, fixed in 4% paraformaldehyde, counterstained with DAPI (0.5 µg/mL), and mounted in FluorSave™.

RNA extraction and quantitative real-time PCR (qPCR)

Total RNA was extracted using the PureLink™ RNA Mini Kit and quantified on a NanoDrop One spectrophotometer (Thermo Fisher Scientific). Equal amounts of RNA were reverse-transcribed using the High-Capacity cDNA Reverse Transcription Kit (Applied Biosystems). Quantitative PCR was performed on a QuantStudio 3 Real-Time PCR System using Power SYBR™ Green PCR Master Mix under the following cycling conditions: 95°C for 10 min, followed by 40 cycles of 95°C for 15 s, 60°C for 60 s, and 72°C for 60 s. Relative gene expression was calculated via the $2^{-\Delta\Delta Ct}$ method normalized to GAPDH as the endogenous control.

Comparative proteomics and bioinformatic analysis

MDA-MB-231 and MDA-MB-468 cells were cultured for 72 h on collagen-coated randomly oriented PCL scaffolds, aligned PCL scaffolds, collagen-coated glass, or tissue culture plastic until reaching ~ 80%

confluence (n = 3 independent biological replicates per group). Cells were detached using Accutase®, washed in PBS, pelleted at 200 × g for 5 min, and precipitated in ice-cold 70% acetone followed by centrifugation at 17,000 × g for 45 min. Protein pellets were solubilized in 4% SDS/Tris-HCl buffer, denatured at 95°C, sonicated, and digested overnight at 37°C with a trypsin/Lys-C protease mix.

Acidified peptides were desalted on Evotips, dried, and resuspended in 0.1% trifluoroacetic acid for liquid chromatography-tandem mass spectrometry (LC-MS/MS) on an Ultimate 3000 nRSLC system coupled to an Orbitrap Q Exactive HF mass spectrometer (Thermo Fisher Scientific) operating in data-independent acquisition (DIA) mode. Raw spectra were processed in DIA-NN against the UniProt human reference proteome using the PG.MaxLFQ label-free quantification algorithm. Proteins with $p < 0.05$ and $|\log_2$ fold change$| > 0.5$ were classified as differentially abundant. Principal component analysis (PCA), volcano plots, and Gene Ontology (GO) Biological Process enrichment analyses were performed to evaluate global proteomic shifts to compare MDA-MB-231 cells on aligned vs glass control.

siRNA formulation and transfection

Cells were transfected 24 h after seeding on standard plasticware or 48 h after seeding on glass and electrospun scaffolds. siRNAs targeting MED27 or EGFR, alongside matched scrambled control siRNA, were delivered using either Lipofectamine™ 2000 or hyaluronan-coated PBAE polyplexes (HAP). HAP nanoparticles were prepared at an amine-to-phosphate (N/P) ratio of 10 and an HA-to-PBAE mass ratio of 0.8, yielding negatively charged, CD44-targeted polyplexes as characterized by Loiudice et al. [25]. In 24-well plates, 42 µL of formulation containing 20 pmol siRNA was added dropwise to 800 µL of complete medium, with a final concentration of 25 nM. In 8-well µ-Slides, 10 µL of formulation containing 5 pmol siRNA was added to 100 µL of medium.

EMT transcriptional array profiling

Exploratory profiling of EMT-associated pathways was conducted using TaqMan™ Array Human Epithelial-Mesenchymal Transition 96-well plates in conjunction with the TaqMan™ Cells-to-CT™ 1-Step Kit (n = 1 array per condition). MDA-MB-231 cells cultured on glass, randomly oriented fibers, or aligned fibers were lysed directly in 50 µL Lysis Solution with DNase I, quenched with Stop Solution, and subjected to one-step RT-qPCR. Across the 12 endogenous candidate genes on the array, GUSB and PGK1 exhibited the highest stability across substrates and were averaged to compute ΔCq values. Relative expression changes were expressed descriptively as $-\Delta\Delta Cq$ ($\log_2$ fold change) relative to untreated cells on glass or matched noncoding HAP controls. Wells failing amplification quality control were excluded.

Gap-closure migration assay

Collective cell migration was evaluated using Culture-Insert 4 Well μ-Dishes (Ibidi). Cells (1×10^4 per well) were seeded and cultured for 24 h prior to siRNA transfection. At 12 h post-transfection, silicone inserts were removed to create standardized cell-free gaps. Phase-contrast images (10× magnification) were captured at 0, 15, 18, 21, and 24 h. Gap closure percentage was quantified in Fiji/ImageJ using a custom macro cross-validated with the Wound_healing_size_tool_update plugin [27].

Statistical analysis

Quantitative data are presented as the mean ± standard deviation (SD) independent biological replicates of n = 7 for qPCR, n = 3 for proteomics and n = 1 for RNA Array experiments. Statistical analyses were conducted in GraphPad Prism using one-way ANOVA followed by Tukey's post-hoc test for single-variable comparisons, or two-way ANOVA with Bonferroni's post-hoc correction for multi-variable comparisons. Statistical significance was defined as $p < 0.05$ (* $p < 0.05$, ** $p < 0.01$, *** $p < 0.001$, **** $p < 0.0001$).

Survival analysis was performed using the publicly available Kaplan–Meier Plotter database [28], which integrates clinical and gene expression data from multiple breast cancer cohorts. Patients were stratified according to MED27 expression, and survival differences were evaluated using Kaplan–Meier curves, hazard ratios, and log-rank tests.

Results

TACS-mimicking fibrous architectures promote EMT-associated transcriptional and proteomic remodeling in TNBC cells

To model the structural transition from isotropic stroma to aligned TACS fibers, MDA-MB-231 cells were cultured on collagen-I-coated randomly oriented or aligned electrospun PCL scaffolds. LIVE/DEAD staining confirmed high cell viability across the fibrous substrates and revealed pronounced topographically driven morphological adaptation (Fig. 1A). Cells on aligned fibers adopted elongated, spindle-shaped morphologies oriented parallel to the fiber axis, characteristic of contact guidance and mesenchymal polarization, whereas cells in unaligned regions remained polygonal or rounded [19]. Confocal microscopy following treatment with AF647-labeled siRNA confirmed robust intracellular internalization of siRNA payloads by cells growing on both random and aligned 3D fiber mats (Fig. 1B), validating the platform for subsequent gene-silencing studies.

We next examined whether fiber architecture directly alters EMT marker expression via RT-qPCR (Fig. 1C). Compared to collagen-coated glass controls, culturing MDA-MB-231 cells on randomly oriented and aligned PCL fibers significantly downregulated the expression of the epithelial adherens junction transcript CDH1 (E-cadherin; $p = 0.0355$ and $p = 0.0411$, respectively).

Conversely, the expression of the mesenchymal intermediate filament gene VIM (vimentin) was significantly elevated on aligned fibers relative to both glass ($p = 0.0036$) and randomly oriented fibers ($p = 0.0299$), demonstrating that fiber anisotropy specifically amplifies mesenchymal commitment. Notably, the stemness- and invasion-associated hyaluronan receptor CD44 was also strongly upregulated on both random ($p = 0.0053$) and aligned ($p = 0.0021$) scaffolds, whereas increases in SNAI1 and EGFR did not reach statistical significance in baseline cultures.

(A) Representative LIVE/DEAD fluorescence microscopy image of MDA-MB-231 cells cultured on aligned electrospun poly(ε-caprolactone) (PCL) fibers for 72 h. Viable cells were stained with calcein AM (green), and dead cells with SYTOX Deep Red (red). Corresponding live and dead controls are shown as insets. Scale bar = 100 μm. **(B)** Representative confocal fluorescence micrographs illustrating the intracellular distribution of Alexa Fluor 647 (AF647)-labeled siRNA (red) in MDA-MB-231 cells cultured on unaligned (top) and aligned (bottom) PCL fibers. Cell nuclei were counterstained with DAPI (blue). Scale bars = 20 μm. **(C)** Relative mRNA expression of epithelial (CDH1/E-cadherin), mesenchymal (VIM/vimentin and SNAI1/Snail), and cell-surface signaling-associated (CD44 and EGFR) markers in MDA-MB-231 cells cultured on collagen-coated glass, unaligned PCL fibers, or aligned PCL fibers. Expression levels were determined by RT-qPCR using the 2^−ΔΔCt method, normalized to GAPDH, and expressed relative to glass controls. Data are presented as mean ± SD ($n = 7$). Statistical significance was assessed by one-way ANOVA followed by Tukey's multiple-comparisons test for each gene. *$p < 0.05$, **$p < 0.01$; only significant comparisons are indicated.

To capture the global molecular response to matrix topography, we performed DIA mass spectrometry proteomics on mesenchymal-like MDA-MB-231 and basal/epithelial-like MDA-MB-468 cells cultured across standard plastic, randomly oriented fibers, and aligned fibers ($n = 3$ per condition). Principal component analysis (PCA) separated the proteomes primarily by cell line identity along PC1 (42.9% of variance) and by substrate architecture along PC2 (17.4% of variance), demonstrating a progressive trajectory from 2D plastic to random and aligned fibrous matrices in both cell lines (Fig. 2A). Gene Ontology (GO) Biological Process enrichment of the differentially abundant proteins revealed strong enrichment for pathways governing intermediate filament cytoskeleton organization, structural cellular adaptation, and peptidase regulation (Fig. 2B). Thus, TACS-mimicking fiber alignment drives coordinated cytoskeletal and proteomic reprogramming alongside classical EMT marker shifts.

(A) Principal component analysis (PCA) of global data-independent acquisition (DIA) proteomic profiles from MDA-MB-231 and MDA-MB-468 cells cultured on glass controls, unaligned PCL fibers, or aligned PCL fibers, together with a HeLa reference. Each point represents an individual biological replicate ($n = 3$ per experimental condition). Principal components 1 and 2 account for 42.9% and 17.4% of the total variance, respectively. The analysis illustrated differences in global protein expression profiles across cell lines and substrate conditions. Arrows indicate observed phenotypical EMT-like changes that form dedicated clusters on PCA. **(B)** Gene Ontology (GO) Biological Process enrichment analysis of the 500 most upregulated proteins identified in MDA-MB-231 cells cultured on aligned PCL fibers relative to glass controls. Enriched terms include intermediate filament organization, intermediate filament cytoskeleton

organization, keratinocyte differentiation, epidermal cell differentiation, skin development, epidermis development, keratinization, multicellular organismal homeostasis, and regulation of peptidase and endopeptidase activity. These functional categories highlight cytoskeletal organization and differentiation-associated processes represented among proteins exhibiting increased abundance under aligned matrix conditions. Bubble size represents the number of genes associated with each GO term, while color indicates the false discovery rate (FDR)-adjusted enrichment significance. The horizontal axis represents the enrichment signal score.

Matrix anisotropy identifies MED27 as an architecture-responsive transcriptional regulator

Inspection of the differential proteomic dataset revealed marked reorganization of proteins involved in mechanotransduction, focal adhesion, and EMT across both TNBC lines. Specifically, culturing cells on aligned fibers altered the standardized abundance of the receptor tyrosine kinase AXL, the cytoskeletal adaptor SORBS2, the desmosomal plaque protein plakophilin-3 (PKP3), VIM, integrin β_1 (ITGB1), and the focal adhesion scaffolding protein paxillin (PXN). In MDA-MB-468 cells, fiber alignment strongly enriched AXL, SORBS2, VIM, ITGB1, and PXN while depleting the epithelial desmosomal component PKP3, consistent with an alignment-induced loss of epithelial cohesion and gain of focal adhesion signaling (Fig. 3A).

Within this mechanoresponsive proteome, Mediator complex subunit 27 (MED27) emerged as one of the most strongly upregulated nuclear regulators on aligned fibers (Fig. 3B). Label-free quantification confirmed that MED27 protein abundance increased significantly on fibrous scaffolds compared to glass controls in MDA-MB-231 cells, peaking on aligned architectures across both MDA-MB-231 and MDA-MB-468 lines (Fig. 3C). Orthogonal validation by RT-qPCR in MDA-MB-231 cells confirmed a parallel increase in MED27 transcript levels on aligned scaffolds (Fig. 3D), indicating that matrix anisotropy upregulates MED27 at the transcriptional level.

(A) Heatmap displaying within-cell-line, protein-wise, standardized z-scores of selected adhesion- and EMT-associated proteins (AXL, SORBS2, PKP3, VIM, ITGB1, and PXN) in MDA-MB-231 and MDA-MB-468 cells cultured on glass, unaligned fibers, and aligned fibers. Color intensity indicates relative protein abundance after standardization within each cell line and protein (n = 3 biological replicates per condition). **(B)** Volcano plot of differential protein abundance in MDA-MB-231 cells cultured on aligned PCL fibers compared with glass controls, based on DIA proteomic analysis. The horizontal axis represents $\log_2$ fold change, and the vertical axis represents $-\log_{10}$ p-value. MED27 is highlighted among proteins exhibiting increased abundance under aligned fiber conditions. **(C)** Relative MED27 protein abundance in MDA-MB-231 and MDA-MB-468 cells across glass, unaligned fiber, and aligned fiber conditions, as determined by DIA proteomics. Data are presented as mean ± SD (n = 3 biological replicates per condition). **(D)** Relative MED27 mRNA expression in MDA-MB-231 cells cultured on glass, unaligned fibers, or aligned fibers, determined by RT-qPCR and expressed relative to glass controls using the 2^−ΔΔCt method. Data are presented as mean ± SD (n = 7). Statistical significance was assessed by

one-way ANOVA followed by Tukey's multiple-comparisons test. Statistical significance is indicated as *p < 0.05, **p < 0.01, ***p < 0.001, and ****p < 0.0001, where applicable.

MED27-targeted silencing reshapes EMT-associated transcriptional programs across distinct matrix environments

To test whether MED27 is functionally required to sustain the alignment-induced transcriptional state, we silenced MED27 in MDA-MB-231 cells cultured on glass, randomly oriented fibers, and aligned fibers and quantified changes in a panel of proliferation and EMT regulatory genes by RT-qPCR (Fig. 4). In control cells, fibrous substrates elevated the expression of MED27, the mitogenic receptor EGFR, the G1/S cell-cycle regulator CCND1 (cyclin D1) (Fig. 4A), VIM, SNAI1, (Fig. 4C) and KLF4, while suppressing CDH1 (Fig. 4B). Transfection with MED27-targeting siRNA significantly depleted MED27 mRNA across all substrates ($p < 0.01$ on random fibers; $p < 0.0001$ on glass and aligned fibers). Crucially, on aligned fibers, MED27 knockdown significantly reversed the matrix-induced upregulation of EGFR ($p < 0.0001$) (Fig. 4A) and VIM ($p < 0.0001$), (Fig. 4C), and modulated CDH1 expression ($p < 0.05$) (Fig. 4B), whereas CCND1, KLF4, and SNAI1 remained largely refractory to acute MED27 depletion on aligned matrices. Notably, the magnitude of EGFR and VIM suppression following MED27 knockdown differed substantially between 2D glass and aligned 3D fibers, demonstrating that the transcriptional dependency on MED27 is shaped by the physical microenvironment.

Targeted RT-qPCR analysis of MDA-MB-231 cells cultured on glass controls, unaligned PCL fibers, or aligned PCL fibers, with or without MED27-targeting siRNA treatment. **(A)** Relative expression of MED27 and the signaling- and proliferation-associated genes EGFR and CCND1 (cyclin D1). **(B)** Relative expression of the epithelial marker CDH1 (E-cadherin) and the transcription factor KLF4. **(C)** Relative expression of the EMT-associated genes SNAI1 (Snail) and VIM (vimentin). Gene expression was determined by the 2^−ΔΔCt method following normalization to the reference gene and is presented relative to the corresponding experimental control. Data are shown as mean ± SD (n = 7). Statistical comparisons between untreated controls and MED27-silenced cells were performed within each substrate condition using two-way ANOVA. Significant differences are indicated by horizontal brackets: *p < 0.05, **p < 0.01, ***p < 0.001, ****p < 0.0001.

Because aligned fibers significantly upregulated CD44 expression (Fig. 1C) to shift into mesenchymal profile, we next evaluated whether MED27 siRNA could be effectively delivered using tumor-targeted, hyaluronan-coated PBAE polyplexes (HAP) designed to engage the CD44 receptor [24, 25]. Using an exploratory TaqMan Human EMT 96-well array (n = 1), we profiled broader transcriptional shifts in MDA-MB-231 cells treated with HAP-formulated siMED27 (HAP-MED27) versus scrambled control polyplexes (HAP-NC) on aligned and unaligned fibers (Fig. 5A). Comparing HAP-MED27 on unaligned versus aligned fibers highlighted strong substrate-dependent divergence across multiple EMT regulators, including EGFR, ZEB1, ZEB2, CTNNB1 (β-catenin), and DSC2 (desmocollin-2). Relative to HAP-NC on aligned fibers, acute HAP-MED27 treatment increased transcripts encoding the tight-junction protein occludin (OCLN;

+1.14 log_2FC) alongside compensatory shifts in ZEB2 (+ 0.92 log_2FC), CTNNB1 (+ 1.03 log_2FC), and TGFB2 (+ 1.13 log_2FC), while suppressing WNT11 (− 0.82 log_2FC) and SMAD2 (− 0.32 log_2FC) expression.

We further compared the transcriptional impact of HAP-mediated MED27 silencing against HAP-mediated EGFR silencing under standard 2D culture conditions (Fig. 5B). Knockdown of EGFR via HAP polyplexes significantly altered CD44, CDH1, VIM, and SNAI1 expression ($p < 0.001$) without affecting MED27 transcript levels, indicating that MED27 operates upstream or independently of EGFR signaling. Conversely, under 2D conditions, HAP-mediated MED27 knockdown induced an unexpected upregulation of EGFR, CD44, and SNAI1 and downregulation of CDH1, contrasting with the suppression observed under 3D fiber conditions. This difference underscores how cationic/polymeric nanoparticle interaction dynamics and 2D vs 3D mechanical constraints can alter acute feedback loops in distinct delivery contexts.

(A) Exploratory TaqMan EMT-related gene expression profiling following treatment with hyaluronic acid-coated polyplexes (HAP) carrying either negative-control siRNA (HAP NC) or MED27-targeting siRNA (HAP MED27). Left: Heatmap of relative expression changes (−ΔΔCq), normalized to GUSB and PGK1 and referenced to untreated cells cultured on glass. Experimental conditions include HAP NC on aligned fibers and HAP MED27 on aligned or unaligned fibers. Gray boxes indicate reactions excluded following amplification quality control. Right: Estimated log_2 fold changes (−ΔΔCq) for HAP MED27 relative to matched HAP NC on aligned fibers. The assay was performed with one biological sample per condition (n = 1); therefore, these data are descriptive and exploratory, and no statistical significance is inferred. **(B)** Targeted RT-qPCR analysis of MED27, EGFR, CD44, CDH1 (E-cadherin), VIM (vimentin), SNAI1 (Snail), and BIRC5 (survivin) in MDA-MB-231 cells treated with HAP formulations containing negative-control, EGFR-targeting, or MED27-targeting siRNA under conventional two-dimensional culture conditions. Relative expression was determined using the 2^−ΔΔCt method. Data are presented as mean ± SD (n = 7). Statistical significance tested via two-way ANOVA is indicated for the comparisons shown: **p < 0.01, ***p < 0.001, ****p < 0.0001. **(C)** Quantification of gap closure over 24 h in MDA-MB-231 cultures left untreated (Blank) or treated with negative-control (CTRL), EGFR-targeting, or MED27-targeting siRNA. Gap closure is expressed as a percentage of the initial cell-free area. Data are presented as mean ± SD (n = 3). This assay measures collective gap closure and does not independently distinguish changes in cell migration from potential effects on proliferation.

MED27-directed intervention impairs TNBC collective migration

Finally, to determine whether the transcriptional perturbations induced by MED27 silencing translate into functional attenuation of cell motility, we performed gap-closure migration assays in MDA-MB-231 cells over 24 h (Fig. 5C). Untreated blank cells and scrambled siRNA treated control cells rapidly migrated into the denuded gap, achieving nearly complete closure (~ 97%) within 24 h. In contrast, cells treated with either EGFR-targeting siRNA (positive migration-inhibition control) or MED27-targeting siRNA exhibited

delayed gap-closure kinetics between 15 h and 24 h. Specifically, MED27 knockdown produced the most pronounced reduction in collective migration across the 24 h time course, reducing final gap closure to ~ 76% (Fig. 5C). Thus, depleting MED27 not only disrupts alignment-associated EMT gene expression (VIM, EGFR) but also functionally impairs TNBC cell migration.

Discussion

While the clinical link between TACS and breast cancer metastasis is firmly established [10, 11], the intracellular mechanisms that couple topographical anisotropy to nuclear gene expression remain incompletely understood. Building upon our previously validated electrospun PCL scaffold platform [19, 20], this study demonstrated that fibrous matrix alignment does not merely guide directional migration via physical confinement but actively reprograms the TNBC proteome and transcriptome. Most notably, we identified MED27 as a novel, topographically responsive coactivator whose abundance scales with fiber alignment and whose silencing blunts key mesenchymal and migratory traits.

Culturing TNBC cells on aligned collagen-coated fibers triggered a classical EMT shift-marked by CDH1 suppression and VIM and CD44 upregulation-accompanied by broad proteomic remodeling of focal adhesion and intermediate filament networks (ITGB1, PXN, SORBS2, AXL, and PKP3). Comparing basal-like MDA-MB-468 cells with mesenchymal-like MDA-MB-231 cells revealed that while both cell lines separate along a defined trajectory on fibrous substrates in PCA space, MDA-MB-468 cells undergo a particularly sharp switch on aligned fibers, losing the desmosomal plaque protein PKP3 while upregulating integrin β_1, paxillin, and the EMT-driving receptor tyrosine kinase AXL. These observations align with contemporary views of EMT as a continuum of hybrid plastic states governed by the interplay between intrinsic cellular phenotype and extrinsic micromechanical cues [7, 8, 16, 17].

A central discovery of our proteomic screen is the robust upregulation of MED27 on aligned fibers across both TNBC cell lines, corroborated at the mRNA level in MDA-MB-231 cells. As a tail/head-associated subunit of the Mediator complex, MED27 bridges sequence-specific transcription factors to the basal RNA polymerase II machinery. Previous studies in standard 2D cultures have shown that MED27 promotes breast cancer progression via KLF4 activation [21] and drives EMT and metastasis in gastric and adrenocortical cancers via Wnt/β-catenin signaling [22, 23]. Our data extend these findings into the realm of cancer mechanobiology, showing that physical fiber alignment acts as an upstream trigger for MED27 accumulation. Given the concurrent enrichment of integrin β_1 and paxillin on aligned scaffolds, we hypothesize that tension-mediated focal adhesion signaling (e.g., via FAK/Src, RhoA/ROCK, or YAP/TAZ nuclear translocation [7, 8, 18]) transcriptionally activates the MED27 locus, positioning MED27 as a nuclear amplifier of mechanotransduction. Clinically, this model is supported by our survival analysis showing that elevated MED27 expression strongly predicts inferior outcomes in breast cancer patients. Kaplan-Meier survival analysis across 4,929 breast carcinoma patients we queried publicly available patient survival datasets demonstrated that high MED27 mRNA expression correlates significantly with reduced relapse- free survival (hazard ratio [HR] = 1.45, 95% CI: 1.30–1.62; log-rank $p = 4.7 \times 10^{-11}$; Fig. 6A) [28]. Integrating our proteomic findings with prior literature [21–23], we formulated a

working model in which topographical alignment engages integrin β_1/FAK/Src and cytoskeletal mechanotransduction cascades to upregulate nuclear MED27, which in turn acts as a transcriptional coactivator supporting EMT, survival, and migratory programs (Fig. 6B).

Functionally, depleting MED27 on aligned fibers significantly reduced EGFR and VIM expression and altered CDH1 levels, demonstrating that MED27 is required to maintain specific branches of the alignment-induced mesenchymal program. Furthermore, MED27 silencing significantly slowed collective migration in gap-closure assays, matching the anti-migratory effect of EGFR knockdown. Importantly, our multisubstrate experiments reveal that the transcriptional consequences of MED27 knockdown are highly context-dependent: several targets (EGFR, VIM, ZEB1/2, CTNNB1) responded differently to MED27 depletion on aligned fibers versus unaligned fibers or flat 2D plastic. This highlights a critical limitation of conventional 2D drug screening, when transcriptional coactivators are induced by 3D matrix topography, their downstream gene networks can only be accurately interrogated within biomimetic microenvironments.

(A) Kaplan–Meier survival analyses comparing patient groups with high and low MED27 expression in breast cancer and triple-negative breast cancer cohorts. Hazard ratios and log-rank p values are displayed. The analyses illustrate the association between MED27 expression and patient outcomes across the indicated cohorts [28]. **(B)** Proposed molecular framework integrating TACS-like matrix anisotropy, cellular mechanotransduction, MED27 expression, and EMT-associated transcriptional regulation. The schematic incorporates established pathways implicated in extracellular matrix signaling and previously reported MED27-associated transcriptional networks. Connections not directly examined in the present study are presented as proposed or literature-supported relationships rather than experimentally established mechanisms.

Finally, our findings offer a rational framework for microenvironment-targeted nanomedicine. Because TACS-like fiber alignment significantly upregulates the hyaluronan receptor CD44 on TNBC cells, coating cationic PBAE/siRNA polyplexes with hyaluronic acid (HAP) provides a dual advantage: shielding the nanoparticle surface charge while promoting active CD44-mediated endocytosis in invasive, mesenchymal-like tumor subpopulations [24–26]. While the present study establishes proof-of-concept for HAP-mediated MED27 delivery *in vitro*, several limitations warrant future investigations. First, direct chromatin immunoprecipitation (ChIP-seq) and epistatic perturbation of FAK or YAP/TAZ are needed to map the exact signaling cascade connecting integrin engagement on aligned fibers to MED27 transcription. Second, the exploratory TaqMan EMT array (n = 1) should be expanded with further biological replicates and protein-level validation to resolve compensatory feedback loops (such as ZEB2 and TGFB2 modulation). Both aspects, however, are outside the scope of this present study. Finally, evaluating HAP-siMED27 biodistribution, target knockdown, and antimetastatic efficacy in orthotopic in vivo TNBC models will be essential to translate this mechanotranscriptional vulnerability into a viable therapeutic strategy.

Conclusion

This study establishes a novel link between tumor-associated extracellular matrix anisotropy and MED27 in TNBC. Using collagen-I-coated electrospun PCL scaffolds that mimic TACS architectures, we show that fiber alignment drives extensive cytoskeletal proteomic remodeling, induces EMT marker shifts, and upregulates MED27 at both the transcript and protein levels. Targeted silencing of MED27 via lipid or CD44-directed hyaluronan-PBAE polyplexes suppresses alignment-induced VIM and EGFR expression and impairs collective TNBC cell migration. Together, our work positions MED27 as a topographically responsive transcriptional hub in TNBC and underscores the value of engineered fibrous biomaterial platforms for discovering and targeting microenvironment-driven cancer vulnerabilities.

Abbreviations

AF647
Alexa Fluor 647
ANOVA
Analysis of variance
ATCC
American Type Culture Collection
BCA
Bicinchoninic acid
CDH1
Cadherin 1 (E-cadherin)
DAPI
4',6-Diamidino-2-phenylindole
DCM
Dichloromethane
DIA
Data-independent acquisition
DMEM
Dulbecco’s modified Eagle medium
DMF
N,N-Dimethylformamide
DMSO
Dimethyl sulfoxide
ECM
Extracellular matrix
EGFR
Epidermal growth factor receptor
EMT
Epithelial–mesenchymal transition
FBS

Fetal bovine serum
FDR
False discovery rate
GO
Gene Ontology
HA
Hyaluronic acid (hyaluronan)
HAP
Hyaluronan-coated poly(β-amino ester) polyplexes
HR
Hazard ratio
KLF4
Krüppel-like factor 4
LC–MS/MS
Liquid chromatography–tandem mass spectrometry
MED27
Mediator complex subunit 27
N/P
Amine-to-phosphate ratio
PBAE
Poly(β-amino ester)
PBS
Phosphate-buffered saline
PCA
Principal component analysis
PCL
Poly(ε-caprolactone)
qPCR
Quantitative polymerase chain reaction
RISC
RNA-induced silencing complex
RT-qPCR
Reverse transcription quantitative polymerase chain reaction
SD
Standard deviation
siRNA
Small interfering RNA
STR
Short tandem repeat
TACS

Tumor-associated collagen signatures
TME
Tumor microenvironment
TNBC
Triple-negative breast cancer
VIM
Vimentin.

Declarations

Ethics approval and consent to participate

None applicable.

Consent for publication

None applicable.

Availability of data and materials

The datasets used and/or analyzed during the current study are available from the corresponding author on reasonable request.

Competing interests

O.M.M. is a co-founder of RNhale GmbH, an SAB member for AMW GmbH, Corden Pharma International GmbH, and Coriolis Pharma GmbH and a consultant for AbbVie Deutschland GmbH and PARI Pharma GmbH on unrelated projects. The remaining authors declare that they have no competing interests.

Funding

This work was funded by the Federal Ministry of Education and Research (BMBF) and the Free State of Bavaria under the Excellence Strategy of the Federal Government and the Länder through the ONE MUNICH project Munich Multiscale Biofabrication (Munich BioFab). Computational and data resources were provided by the Leibniz Supercomputing Centre (www.lrz.de).

Authors' contributions

M.M. led the coordination and experimental design, performed electrospinning, proteomic data analysis, EMT-related gene expression profiling, and RT-qPCR experiments, and was responsible for data interpretation, visualization, and preparation of the original manuscript. G.L. played a key role in the development and fabrication of electrospun fibrous scaffolds, optimization and preparation of HA-PBAE (HAP) polyplex formulations, and their cellular evaluation, including siRNA internalization and gap-closure assays. G.L. also contributed to cell culture and sample preparation for proteomic and gene

expression analyses. E.T. contributed primarily to the molecular characterization of EMT-associated responses through gene expression array profiling and RT-qPCR analyses, alongside supporting cell culture, polyplex preparation, and gap-closure experiments. I.F. and A.I. contributed their expertise in mass spectrometry-based proteomics, including LC–MS/MS analysis and proteomic data acquisition. O.M.M., as the principal investigator and corresponding author, conceived and oversaw the broader research direction, secured funding, provided scientific leadership and critical guidance throughout the study, and critically reviewed and revised the manuscript. All authors read and approved the final manuscript.

The authors further disclose that ChatGPT was used to improve the conciseness and language of the original manuscript. The final text was reviewed and approved by the authors.

Acknowledgements

AI-assisted language editing: ChatGPT (OpenAI) was used to improve the conciseness and English-language clarity of the authors' original manuscript text. The authors reviewed and approved the final content and take full responsibility for its accuracy.

References

1. Sung H, Filho AM, Laversanne M, Ferlay J, Siegel RL, Soerjomataram I, Jemal A, Bray F. Global cancer statistics 2024: GLOBOCAN estimates of incidence and mortality worldwide for 34 cancers in 186 countries. CA Cancer J Clin. 2026Jul-Aug;76(4):e70090. PMID: 42417444; PMCID: PMC13343830.
2. World Health Organization. Breast cancer. 3. Jul 2026. https://www.who.int/news-room/fact-sheets/detail/breast-cancer. Accessed 3 Nov 2026.
3. Xiong X, Zheng L-W, Ding Y, et al. Breast Cancer: Pathogenesis and Treatments. Signal Transduct Target Ther. 2025;10:1–33. 10.1038/s41392-024-02108-4.
4. Rakha EA, Tse GM, Quinn CM. An Update on the Pathological Classification of Breast Cancer. Histopathology. 2023;82:5–16. 10.1111/his.14786.
5. Kesireddy M, Elsayed L, Shostrom VK, et al. Overall Survival and Prognostic Factors in Metastatic Triple-Negative Breast Cancer: A National Cancer Database Analysis. Cancers. 2024;16:1791. 10.3390/cancers16101791.
6. Butcher DT, Alliston T, Weaver VM. A Tense Situation: Forcing Tumour Progression. Nat Rev Cancer. 2009;9:108–22. 10.1038/nrc2544.
7. Di X, Gao X, Peng L, et al. Cellular Mechanotransduction in Health and Diseases: From Molecular Mechanism to Therapeutic Targets. Signal Transduct Target Ther. 2023;8:1–32. 10.1038/s41392-023-01501-9.
8. Horta CA, Doan K, Yang J. Mechanotransduction Pathways in Regulating Epithelial-Mesenchymal Plasticity. Curr Opin Cell Biol. 2023;85:102245. 10.1016/j.ceb.2023.102245.

9. Elosegui-Artola A, Gupta A, Najibi AJ, et al. Matrix Viscoelasticity Controls Spatiotemporal Tissue Organization. Nat Mater. 2023;22:117–27. 10.1038/s41563-022-01400-4.
10. Conklin MW, Eickhoff JC, Riching KM, et al. Aligned Collagen Is a Prognostic Signature for Survival in Human Breast Carcinoma. Am J Pathol. 2011;178:1221–32.
11. Xi G, Guo W, Kang D, et al. Large-scale tumor-associated collagen signatures identify high-risk breast cancer patients. Theranostics. 2021;11:3229–43. 10.7150/thno.55921.
12. Riching KM, Cox BL, Salick MR, et al. 3D Collagen Alignment Limits Protrusions to Enhance Breast Cancer Cell Persistence. Biophys J. 2014;107:2546–58. 10.1016/j.bpj.2014.10.035.
13. Ray A, Slama ZM, Morford RK, Madden SA, Provenzano PP. Enhanced Directional Migration of Cancer Stem Cells in 3D Aligned Collagen Matrices. Biophys J. 2017;112:1023–36. 10.1016/j.bpj.2017.01.007.
14. Provenzano PP, Inman DR, Eliceiri KW, Trier SM, Keely PJ. Contact Guidance Mediated Three-Dimensional Cell Migration Is Regulated by Rho/ROCK-Dependent Matrix Reorganization. Biophys J. 2008;95:5374–84. 10.1529/biophysj.108.133116.
15. Ray A, Morford RK, Ghaderi N, Odde DJ, Provenzano PP. Dynamics of 3D Carcinoma Cell Invasion into Aligned Collagen. Integr Biol. 2018;10:100–12. 10.1039/c7ib00152e.
16. Yang J, Antin P, Berx G, et al. Guidelines and Definitions for Research on Epithelial–Mesenchymal Transition. Nat Rev Mol Cell Biol. 2020;21:341–52. 10.1038/s41580-020-0237-9.
17. Ghafoor S, Garcia E, Jay DJ, Persad S. Molecular Mechanisms Regulating Epithelial Mesenchymal Transition (EMT) to Promote Cancer Progression. Int J Mol Sci. 2025;26:4364. 10.3390/ijms26094364.
18. Korol A, Taiyab A, West-Mays JA. RhoA/ROCK Signaling Regulates TGFβ-Induced Epithelial-Mesenchymal Transition of Lens Epithelial Cells through MRTF-A. Mol Med. 2016;22:713–23. 10.2119/molmed.2016.00041.
19. Isert L, Passi M, Freystetter B, et al. Cellular EMT-status governs contact guidance in an electrospun TACS-mimicking in vitro model. Mater Today Bio. 2025;30:101401. 10.1016/j.mtbio.2024.101401.
20. Isert L, Mehta A, Loiudice G, Oliva A, Roidl A, Merkel OM. An In Vitro Approach to Model EMT in Breast Cancer. Int J Mol Sci. 2023;24:7757. 10.3390/ijms24097757.
21. Wang R, Yu W, Zhu T, et al. MED27 plays a tumor-promoting role in breast cancer progression by targeting KLF4. Cancer Sci. 2023;114:2277–92. 10.1111/cas.15757.
22. Han X, Liu H, Tang X, Zhao Y. Knockdown of mediator complex subunit 27 suppresses gastric cancer cell metastasis and angiogenesis via Wnt/β-catenin pathway. Tissue Cell. 2022;79:101973. 10.1016/j.tice.2022.101973.
23. He H, Dai J, Yang X, Wang X, Sun F, Zhu Y. Silencing of MED27 Inhibits Adrenal Cortical Carcinogenesis by Targeting the Wnt/β-Catenin Signaling Pathway and the Epithelial-Mesenchymal Transition Process. Biol Chem. 2018;399:593–602. 10.1515/hsz-2017-0304.

24. Isert L, Gialdini I, Ngo TMH, Loiudice G, Lamb DC, Merkel OM. Upholding Hyaluronic Acid's Multi-Functionality for Nucleic Acid Drug Delivery to Target EMT in Breast Cancer. Nanoscale. 2025. 10.1039/D5NR00808E.
25. Loiudice G, Molbay M, Kromer APE, Steinegger KM, Kugler C, Bocanegra L, Sami H, Ogris M, Merkel OM. Hyaluronan-coated Polymeric Nanoparticles for Targeted siRNA Delivery to Metastatic Breast Cancer. Manuscript submitted.
26. Kromer APE, et al. Design of Experiments Grants Mechanistic Insights into the Synthesis of Spermine-Containing PBAE Copolymers. ACS Appl Mater Interfaces. 2024;16(29):37545. 10.1021/acsami.4c06079.
27. Suarez-Arnedo A, Torres Figueroa F, Clavijo C, Arbeláez P, Cruz JC, Muñoz-Camargo C. An image J plugin for the high throughput image analysis of in vitro scratch wound healing assays. PLoS ONE. 2020;15(7):e0232565. 10.1371/journal.pone.0232565.
28. Kaplan–Meier Plotter. Breast cancer survival analysis. https://kmplot.com/analysis/index.php?p=service. Accessed 3 Nov 2026.

Figures

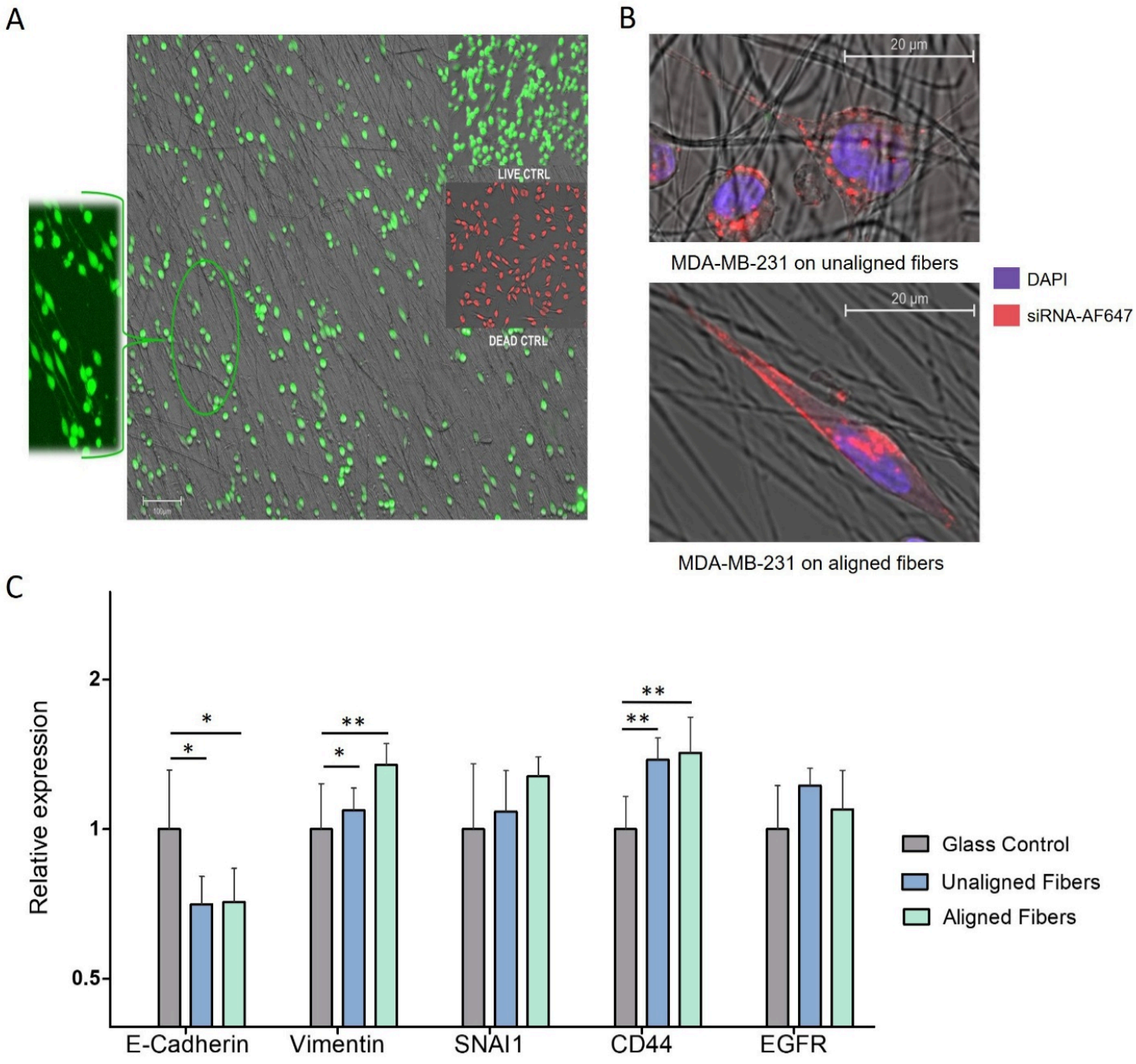


Figure 1

Matrix anisotropy modulates EMT-associated gene expression and siRNA uptake in triple-negative breast cancer cells.

(A) Representative LIVE/DEAD fluorescence microscopy image of MDA-MB-231 cells cultured on aligned electrospun poly(ε-caprolactone) (PCL) fibers for 72 h. Viable cells were stained with calcein AM (green), and dead cells with SYTOX Deep Red (red). Corresponding live and dead controls are shown as insets. Scale bar = 100 µm. **(B)** Representative confocal fluorescence micrographs illustrating the intracellular distribution of Alexa Fluor 647 (AF647)-labeled siRNA (red) in MDA-MB-231 cells cultured on unaligned (top) and aligned (bottom) PCL fibers. Cell nuclei were counterstained with DAPI (blue). Scale bars = 20

µm. **(C)** Relative mRNA expression of epithelial (CDH1/E-cadherin), mesenchymal (VIM/vimentin and SNAI1/Snail), and cell-surface signaling-associated (CD44 and EGFR) markers in MDA-MB-231 cells cultured on collagen-coated glass, unaligned PCL fibers, or aligned PCL fibers. Expression levels were determined by RT-qPCR using the 2^−ΔΔCt method, normalized to GAPDH, and expressed relative to glass controls. Data are presented as mean ± SD (n = 7). Statistical significance was assessed by one-way ANOVA followed by Tukey's multiple-comparisons test for each gene. *p < 0.05, **p < 0.01; only significant comparisons are indicated.

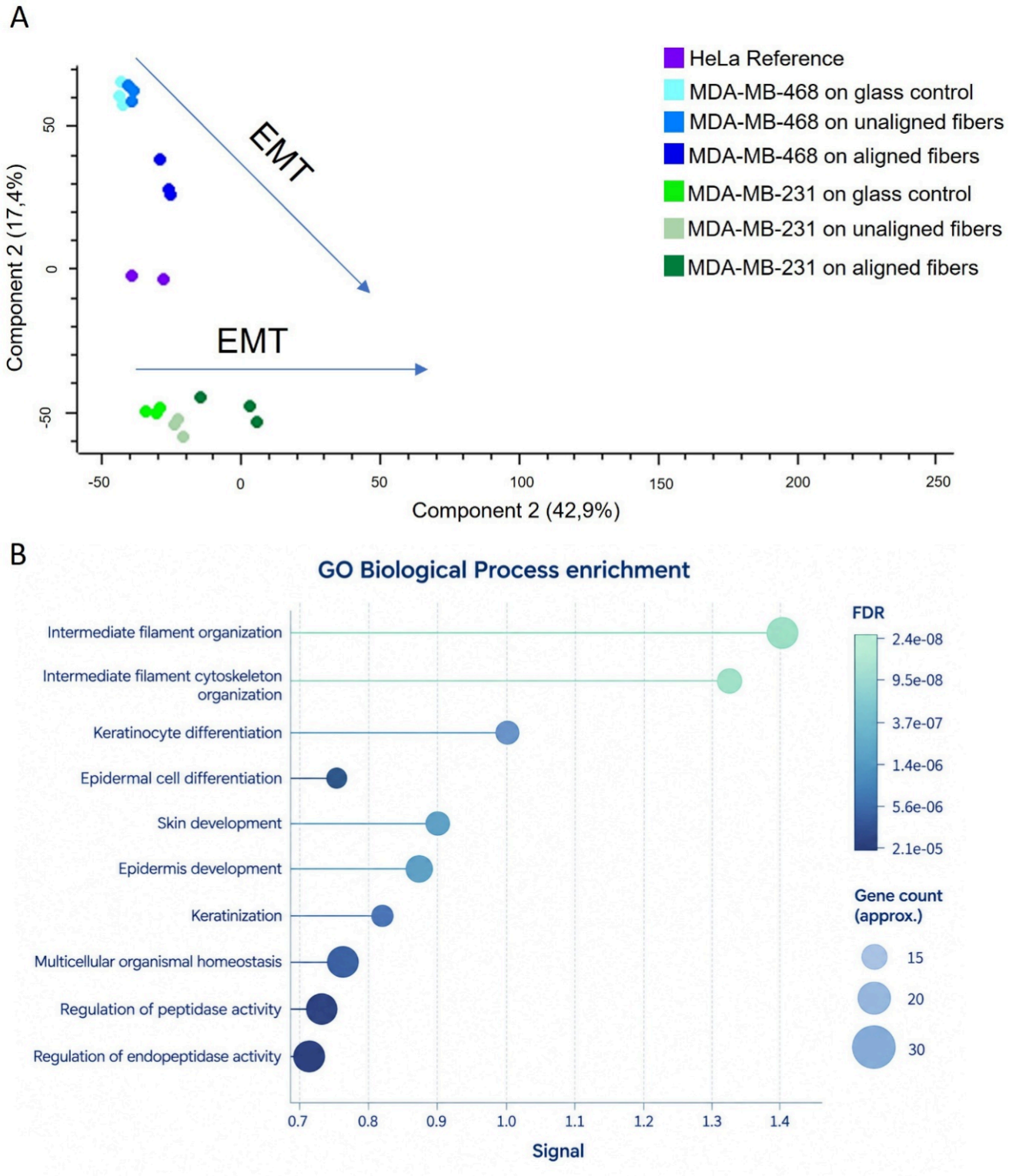


Figure 2

Matrix architecture is associated with distinct proteomic profiles in TNBC cells.

(A) Principal component analysis (PCA) of global data-independent acquisition (DIA) proteomic profiles from MDA-MB-231 and MDA-MB-468 cells cultured on glass controls, unaligned PCL fibers, or aligned PCL fibers, together with a HeLa reference. Each point represents an individual biological replicate (n = 3 per experimental condition). Principal components 1 and 2 account for 42.9% and 17.4% of the total variance, respectively. The analysis illustrated differences in global protein expression profiles across cell lines and substrate conditions. Arrows indicate observed phenotypical EMT-like changes that form dedicated clusters on PCA. **(B)** Gene Ontology (GO) Biological Process enrichment analysis of the 500 most upregulated proteins identified in MDA-MB-231 cells cultured on aligned PCL fibers relative to glass controls. Enriched terms include intermediate filament organization, intermediate filament cytoskeleton organization, keratinocyte differentiation, epidermal cell differentiation, skin development, epidermis development, keratinization, multicellular organismal homeostasis, and regulation of peptidase and endopeptidase activity. These functional categories highlight cytoskeletal organization and differentiation-associated processes represented among proteins exhibiting increased abundance under aligned matrix conditions. Bubble size represents the number of genes associated with each GO term, while color indicates the false discovery rate (FDR)-adjusted enrichment significance. The horizontal axis represents the enrichment signal score.

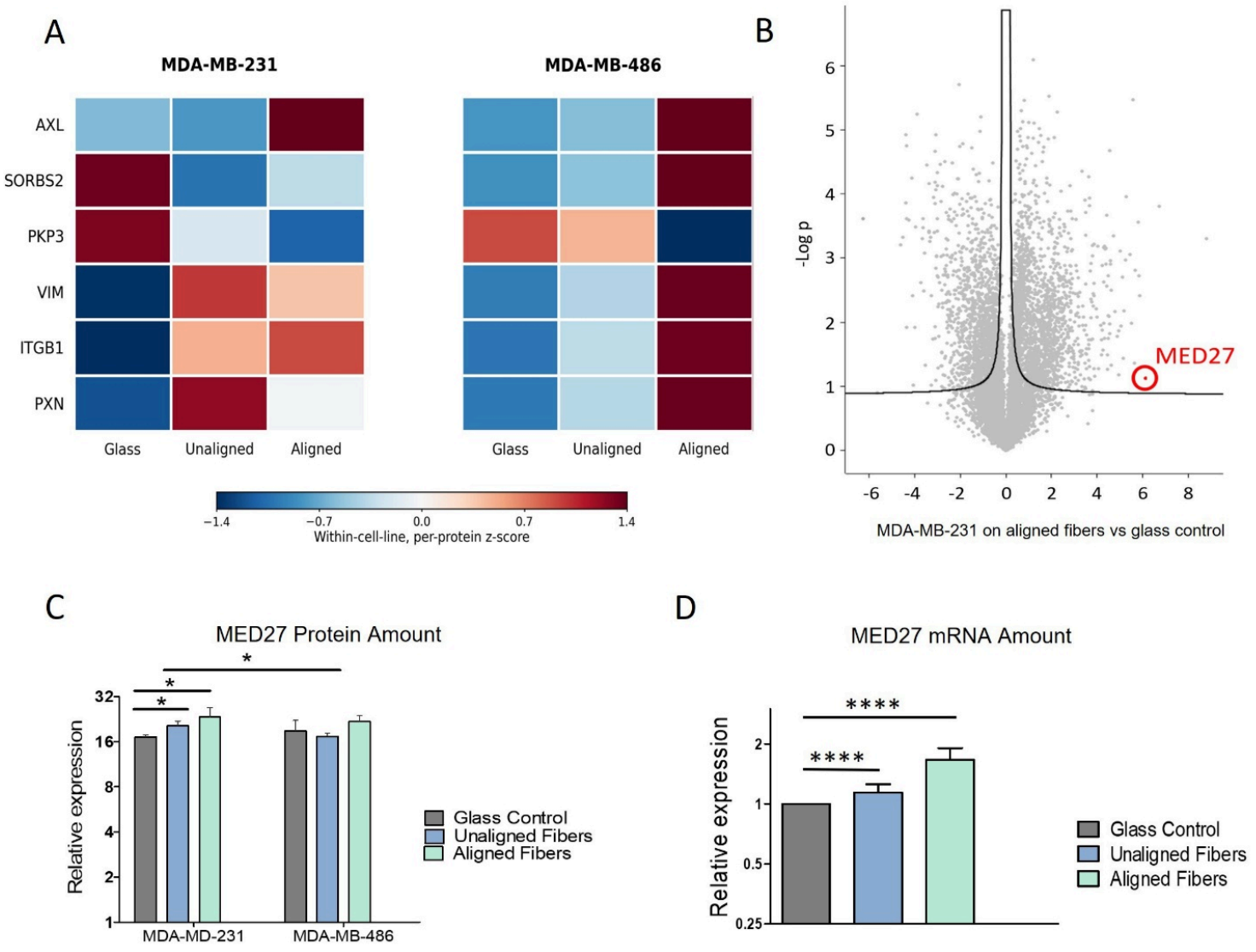


Figure 3

Matrix anisotropy is associated with increased MED27 expression in TNBC cells.

(A) Heatmap displaying within-cell-line, protein-wise, standardized z-scores of selected adhesion- and EMT-associated proteins (AXL, SORBS2, PKP3, VIM, ITGB1, and PXN) in MDA-MB-231 and MDA-MB-468 cells cultured on glass, unaligned fibers, and aligned fibers. Color intensity indicates relative protein abundance after standardization within each cell line and protein (n = 3 biological replicates per condition). **(B)** Volcano plot of differential protein abundance in MDA-MB-231 cells cultured on aligned PCL fibers compared with glass controls, based on DIA proteomic analysis. The horizontal axis represents $\log_2$ fold change, and the vertical axis represents $-\log_{10}$ p-value. MED27 is highlighted among proteins exhibiting increased abundance under aligned fiber conditions. **(C)** Relative MED27 protein abundance in MDA-MB-231 and MDA-MB-468 cells across glass, unaligned fiber, and aligned fiber conditions, as determined by DIA proteomics. Data are presented as mean ± SD (n = 3 biological replicates per condition). **(D)** Relative MED27 mRNA expression in MDA-MB-231 cells cultured on glass, unaligned fibers, or aligned fibers, determined by RT-qPCR and expressed relative to glass controls using

the 2^−ΔΔCt method. Data are presented as mean ± SD (n = 7). Statistical significance was assessed by one-way ANOVA followed by Tukey's multiple-comparisons test. Statistical significance is indicated as *p < 0.05, **p < 0.01, ***p < 0.001, and ****p < 0.0001, where applicable.

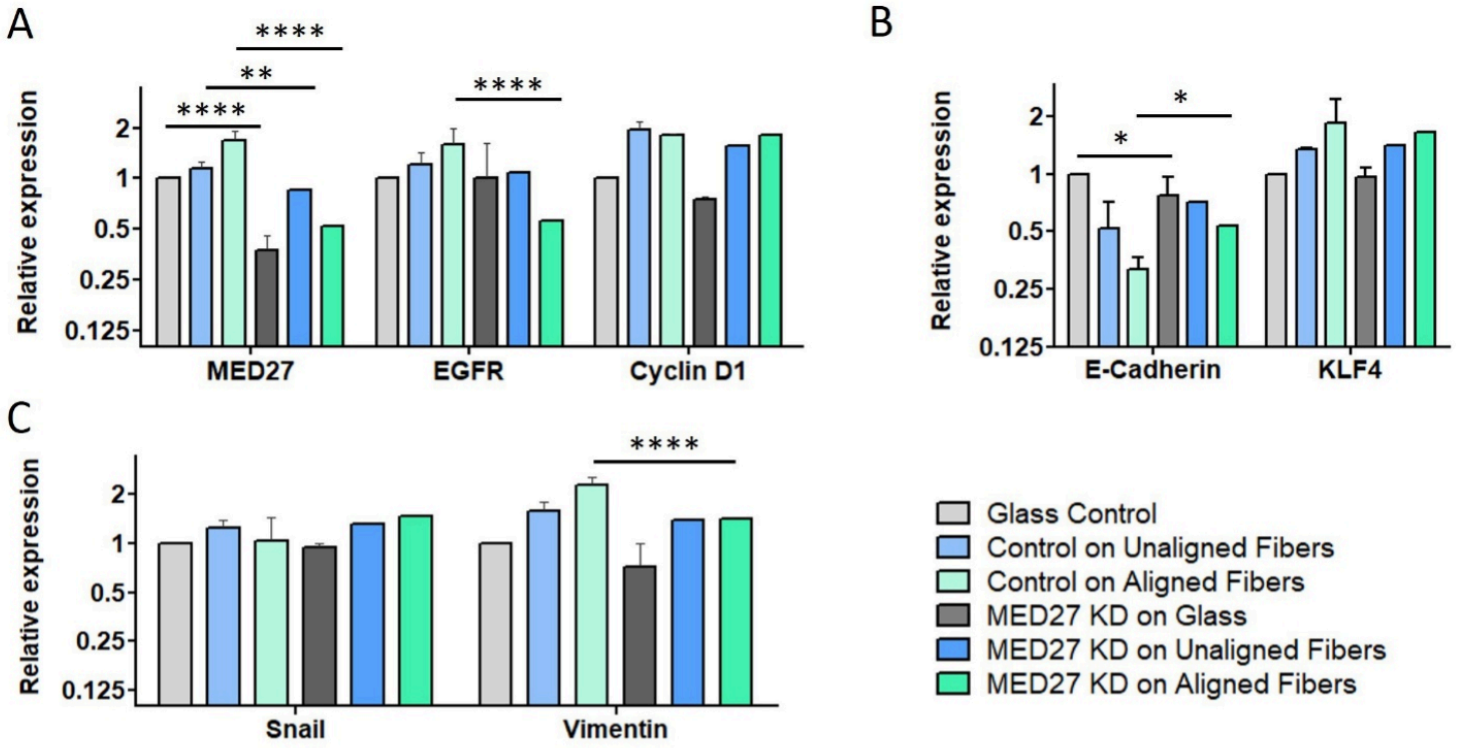


Figure 4

MED27 silencing alters EMT-associated transcriptional responses in MDA-MB-231 cells across distinct matrix architectures.

Targeted RT-qPCR analysis of MDA-MB-231 cells cultured on glass controls, unaligned PCL fibers, or aligned PCL fibers, with or without MED27-targeting siRNA treatment. **(A)** Relative expression of MED27 and the signaling- and proliferation-associated genes EGFR and CCND1 (cyclin D1). **(B)**Relative expression of the epithelial marker CDH1 (E-cadherin) and the transcription factor KLF4. **(C)** Relative expression of the EMT-associated genes SNAI1 (Snail) and VIM (vimentin). Gene expression was determined by the 2^−ΔΔCt method following normalization to the reference gene and is presented relative to the corresponding experimental control. Data are shown as mean ± SD (n = 7). Statistical comparisons between untreated controls and MED27-silenced cells were performed within each substrate condition using two-way ANOVA. Significant differences are indicated by horizontal brackets: *p < 0.05, **p < 0.01, ***p < 0.001, ****p < 0.0001.

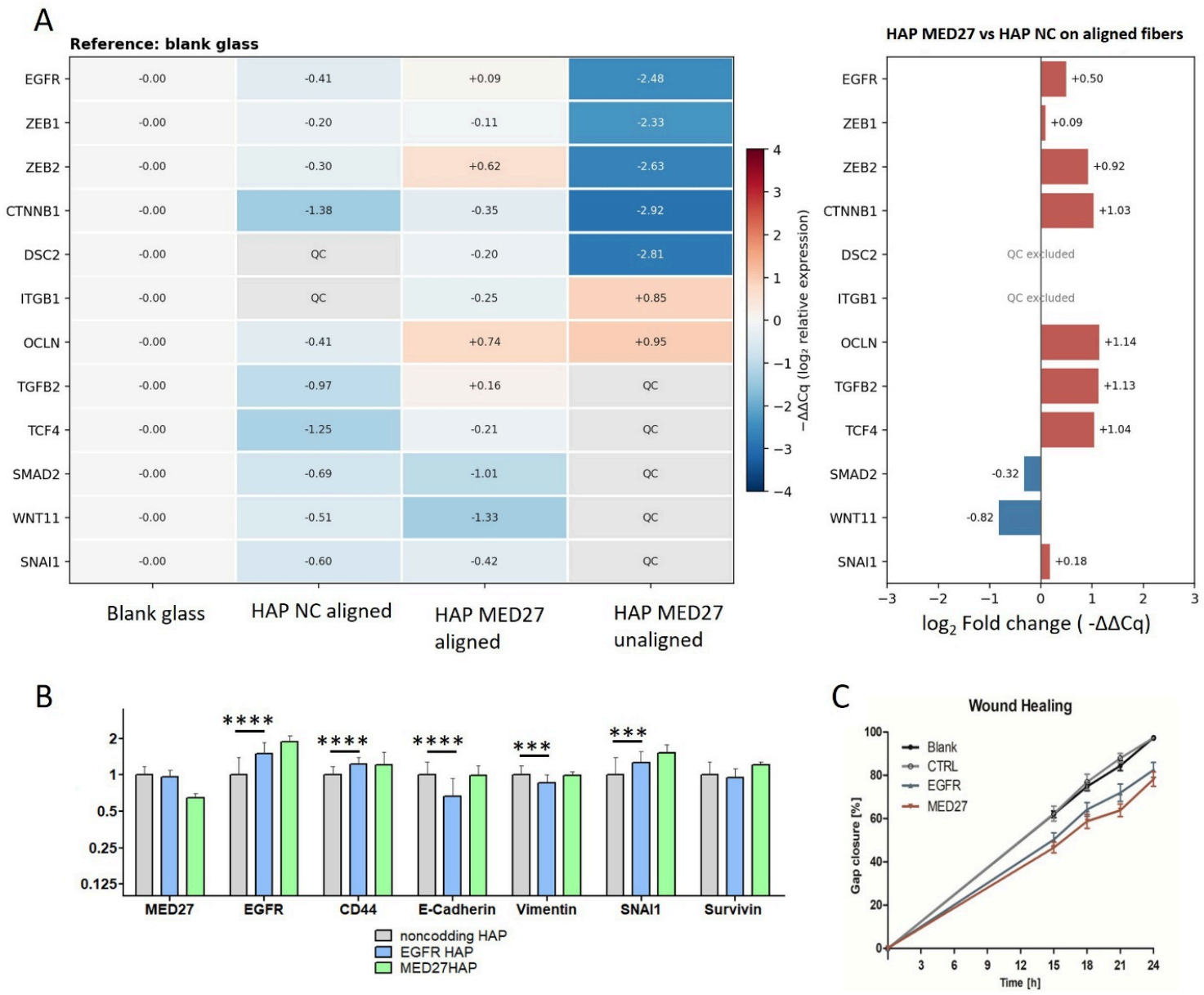


Figure 5

HA-coated polyplex-mediated siRNA delivery modulates EMT-associated gene expression and cell gap closure in MDA-MB-231 cells.

(A) Exploratory TaqMan EMT-related gene expression profiling following treatment with hyaluronic acid-coated polyplexes (HAP) carrying either negative-control siRNA (HAP NC) or MED27-targeting siRNA (HAP MED27). Left: Heatmap of relative expression changes (−ΔΔCq), normalized to GUSB and PGK1 and referenced to untreated cells cultured on glass. Experimental conditions include HAP NC on aligned fibers and HAP MED27 on aligned or unaligned fibers. Gray boxes indicate reactions excluded following amplification quality control. Right: Estimated $\log_2$ fold changes (−ΔΔCq) for HAP MED27 relative to matched HAP NC on aligned fibers. The assay was performed with one biological sample per condition (n = 1); therefore, these data are descriptive and exploratory, and no statistical significance is inferred. **(B)** Targeted RT-qPCR analysis of MED27, EGFR, CD44, CDH1 (E-cadherin), VIM (vimentin), SNAI1 (Snail),

and BIRC5 (survivin) in MDA-MB-231 cells treated with HAP formulations containing negative-control, EGFR-targeting, or MED27-targeting siRNA under conventional two-dimensional culture conditions. Relative expression was determined using the 2^−ΔΔCt method. Data are presented as mean ± SD (n = 7). Statistical significance tested via two-way ANOVA is indicated for the comparisons shown: **p < 0.01, ***p < 0.001, ****p < 0.0001. **(C)**Quantification of gap closure over 24 h in MDA-MB-231 cultures left untreated (Blank) or treated with negative-control (CTRL), EGFR-targeting, or MED27-targeting siRNA. Gap closure is expressed as a percentage of the initial cell-free area. Data are presented as mean ± SD (n = 3). This assay measures collective gap closure and does not independently distinguish changes in cell migration from potential effects on proliferation.

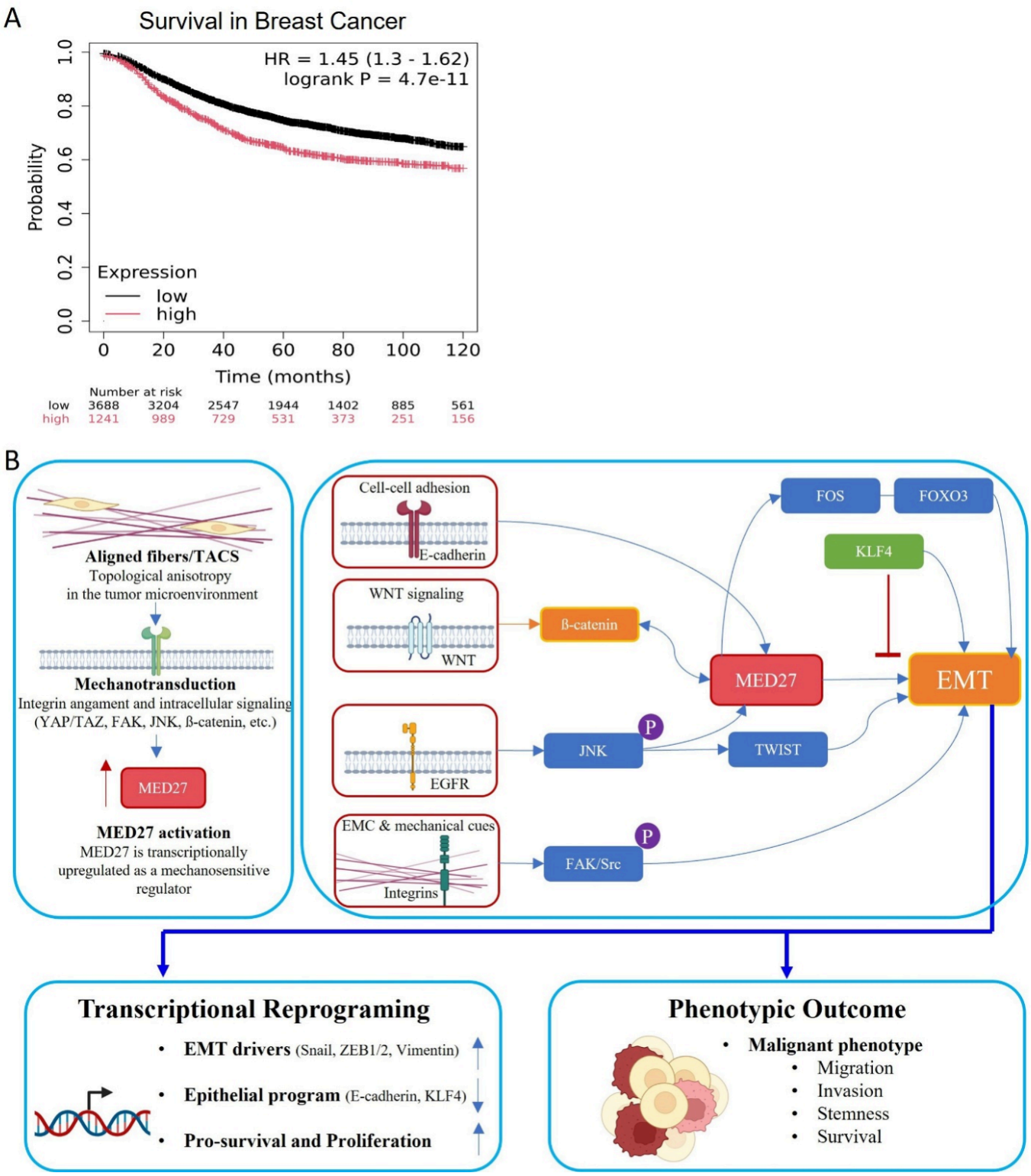


Figure 6

Clinical effect of MED27 overexpression and suggested framework.

(A) Kaplan–Meier survival analyses comparing patient groups with high and low MED27 expression in breast cancer and triple-negative breast cancer cohorts. Hazard ratios and log-rank p values are displayed. The analyses illustrate the association between MED27 expression and patient outcomes

across the indicated cohorts [28]. **(B)** Proposed molecular framework integrating TACS-like matrix anisotropy, cellular mechanotransduction, MED27 expression, and EMT-associated transcriptional regulation. The schematic incorporates established pathways implicated in extracellular matrix signaling and previously reported MED27-associated transcriptional networks. Connections not directly examined in the present study are presented as proposed or literature-supported relationships rather than experimentally established mechanisms.